Electronic Supplementary Material (ESI) for Soft Matter.

Supplementary Information

Hydrophobicity of surface-immobilised molecules influences architectures formed via interfacial self-assembly of nucleoside-based gelators

Maria Galini Faidra Angelerou[1], Bin Yang[1], Tom Arnold[2-5], Jonathan Rawle[2], Maria Marlow*[1] and Mischa Zelzer*[1]

[1] *Department of Pharmacy, University of Nottingham, Nottingham, NG2 7RD, United Kingdom*

[2] *I07 Diamond Light Source Ltd, Harwell Science and Innovation Campus, Didcot, Oxfordshire, OX11 0DE, United Kingdom*

[3] *European Spallation Source ERIC, P.O Box 176, SE-221 00 Lund, Sweden*

[4] *STFC, Rutherford Appleton Laboratory, Chilton Didcot, OX11 0QX , UK*

[5] *Department of Chemistry, University of Bath, Claverton Down, Bath BA2 7AY, UK*

Email: maria.marlow@nottingham.ac.uk , mischa.zelzer@nottingham.ac.uk

Contents

1) Structures of nucleoside-based gelators

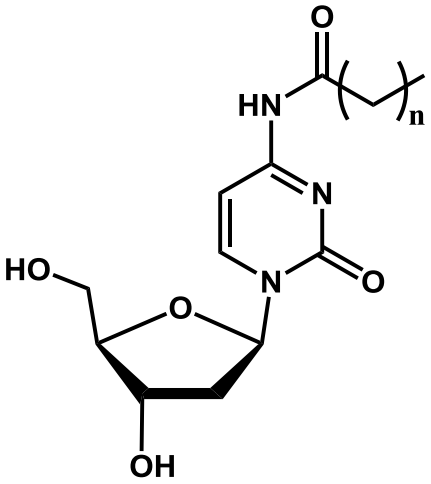

Figure S1: Structure of the nucleoside-based gelator with different alkyl chain lengths; C8-dCyt (n=6 carbon atoms), C10-dCyt (n=8 carbon atoms) , C12-dCyt (n=10 carbon atoms) and C14-dCyt (n=12 carbon atoms)).

2) AFM images of all the surfaces

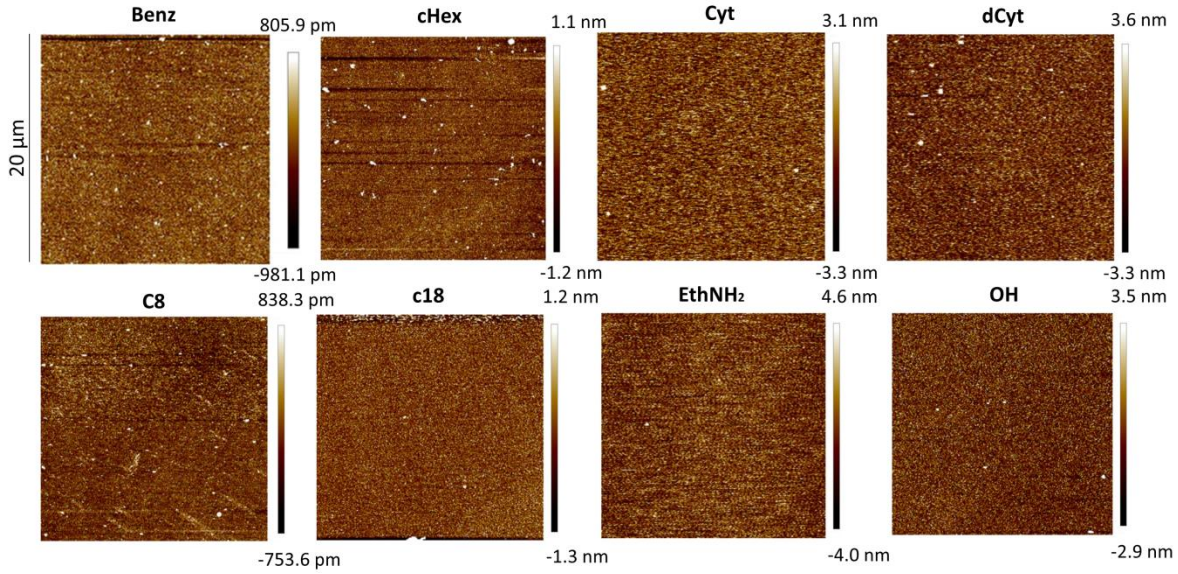

Figure S2: AFM images of the differently modified surfaces. Each image represents a square with dimensions of 20 µm x 20 µm. Different surface chemistries; alkyl chains containing 8 or 18 carbons (C8 and C18), ethylamine ($EtNH_2$), deoxy-cytidine (dCyt), cytidine (Cyt) cyclohexyl (cHex) and benzyl (Benz) groups and piranha cleaned (OH).

3) Surface properties

Table S1: Values for characteristic properties of different surfaces derived from experimental measurements. Roughness average (R_a) and Root mean square roughness (R_q) were determined experimentally through Atomic Force Microscopy (AFM) images (figure S1) and Water Contact Angle(WCA) determined experimentally.

surface \ property	R_q (nm)	R_a (nm)	WCA (°)
Benz	0.391 ± 0.093	0.195 ± 0.005	57.6 ± 1.2
cHex	0.676 ± 0.078	0.26 ± 0.021	55.1 ± 1.9
C8	0.346 ± 0.035	0.183 ± 0.006	74.7 ± 1.6
C18	0.306 ± 0.078	0.228 ± 0.064	72.8 ± 2.7
$EtNH_2$	0.904 ± 0.275	0.659 ± 0.303	67.3 ± 6.5
dCyt	1.041 ± 0.092	0.709 ± 0.081	34.5 ± 1.6
Cyt	0.698 ± 0.237	0.548 ± 0.208	35.5 ± 1.2
OH	1.031 ± 0.167	0.717 ± 0.059	4.7 ± 0.7

4) AFM images of xerogels on all the surfaces

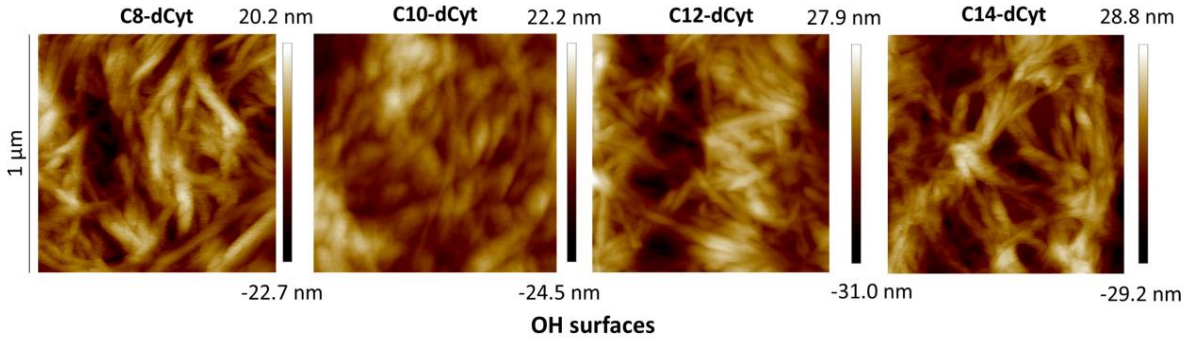

Figure S3: AFM images of dry gels on different surfaces; gels formed by four gelators with different alkyl chain lengths on OH surfaces.

5) Time-resolved GIWAXS and GISAXS

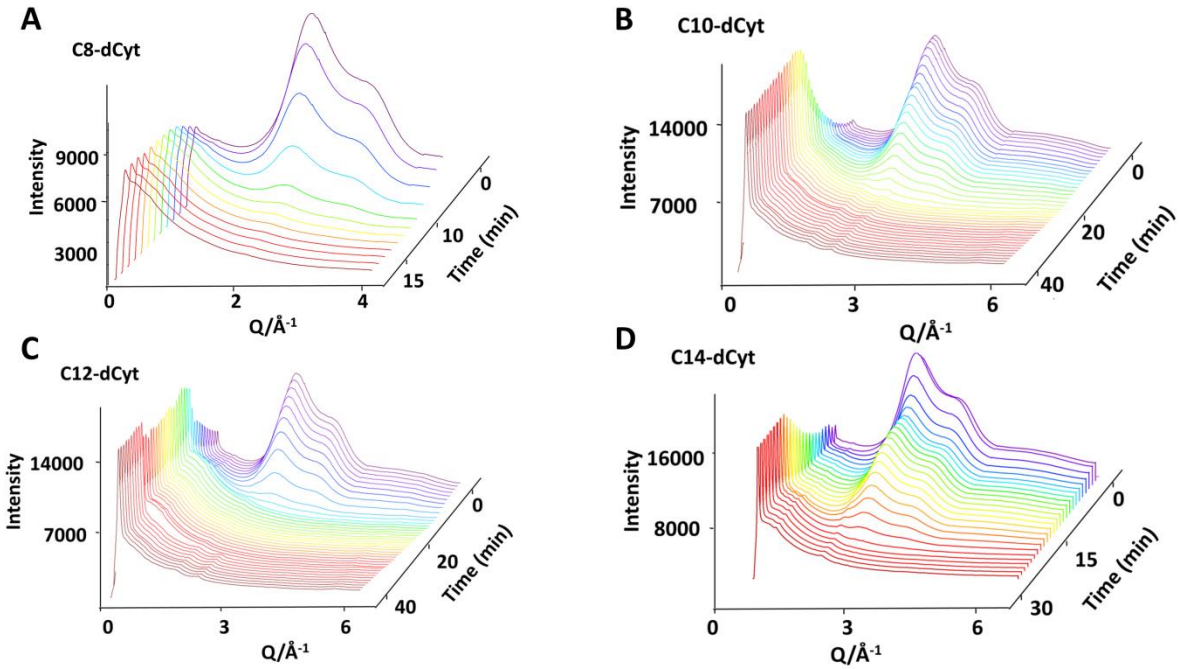

Figure S4: Time resolve GIWAXS pattern of gels formed by for four different cytosine based gelators with varying aliphatic chain lengths on clean silicon wafers; (A) C8-dCyt, (B) C10-dCyt, (C) C12-dCyt and (D) C14-dCyt.

Table S2: Definitions of fibre unit and fibre bundle as used in this work.

Unit fibre 	First-order cylindrical structure that consists of oriented gelator molecules; the lipophilic alkyl chain of each molecule is towards the core of the fibre whereas the hydrophilic sugar points towards the external surface
Fibre bundle 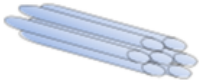	Higher-order cylindrical structures that consists of unit fibres associated together

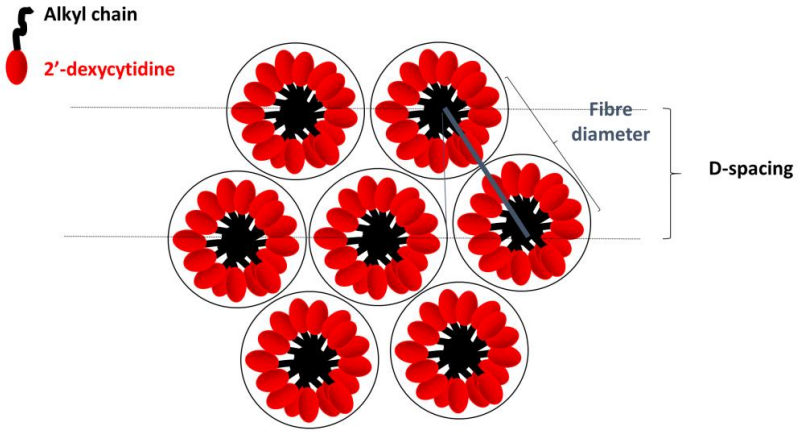

Figure S5: Proposed hexagonal packing for unit fibres. D-spacing determined experimentally is presented and the fibre diameter is calculated trigonometrically as proposed.

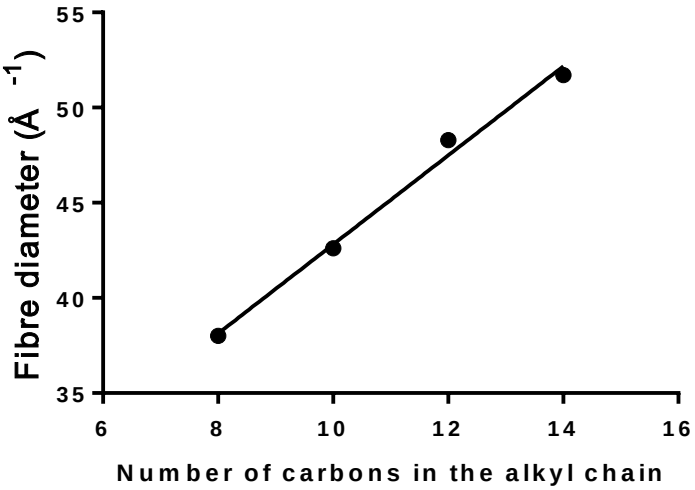

Figure S6: Fibre diameter against number of carbons in the alkyl chain (R^2=0.9915). Fibre diameter values were determined through the GIWAXS patterns as explained in Figure S5.

Table S3: Reflection peaks, Q-ratio, D-spacing and assignments to the fibre structures of thin gel films of the four gelators on piranha cleaned silicon wafers in GIWAXS setup.

Reflection peaks ($Å^{-1}$)	Q ratio	D-spacing ($Å^{-1}$)	Assignment to fiber structures
0.19, 0.38 **(C8-dCyt)** 0.17, 0.35, 0.53, 0.68, 1.07 **(C10-dCyt)** 0.15, 0.3, 0.45, 0.6 **(C12-dCyt)** 0.14, 0.28, 0.42 **(C14-dCyt)**	1:2 1:2:3:4:6 1:2:3:4 1:2:3	33 36.9 41.8 44.8	D-spacing related to the hexagonal packing
0.55 **(for all gelators)**		11.4	D-spacing related to the hexagonal packing
1.53 **(for all gelators)**		4.1	the N-H-O bond spacing of the gelator along the fiber axis or the distance between the stacked nucleobases

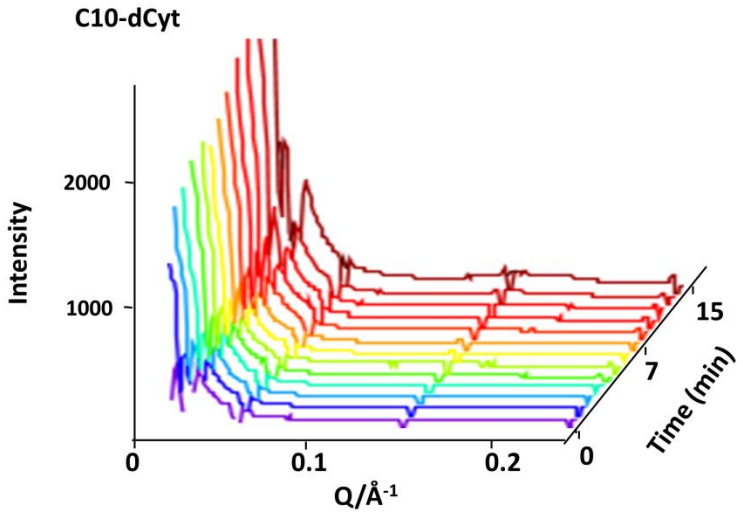

Figure S7: Time resolved GISAXS pattern of gels formed by C10-dCyt on a clean silicon wafer. Data points between 0.030 $Å^{-1}$ - 0.048 $Å^{-1}$ and 0.062 $Å^{-1}$ - 0.074 $Å^{-1}$,0.156 $Å^{-1}$ - 0.158 $Å^{-1}$ 0.246 $Å^{-1}$ - 0.247 $Å^{-1}$ are missing due to masking by the reflective beam-stop and the spaces between the detector plates, respectively.

The ability of single fibers in supramolecular gels to associate with each other and form higher order structures such as helices, ribbons, twists and bundles is well documented.[1-4] In order to explore association of fibers formed by the four different nucleoside based gelators, we used GISAXS. An example of a GISAXS time-resolved pattern is presented in SI, Figure S7. A broad peak with a maximum intensity approximately at Q=0.19 $Å^{-1}$, 0.170 $Å^{-1}$, 0.15 $Å^{-1}$ and

0.140 $Å^{-1}$ for the C8-dCyt, C10-dCyt, C12-dCyt and C14-dCyt, respectively, develops for all gel samples during drying (SI, Figure S8). As presented in SI, Figure S9 due to the peak distortion as a result of the 2D detector gaps, the intensity maxima are hard to be accurately determined, there is thought a clear peak shift in agreement with the trend followed in the GIWAXS setup. These peaks correspond to the lowest Q peak observed in the GIWAXS experiment. This confirms that these peaks are not artifacts introduced by the proximity of the beam stopper.

The first collected pattern was fitted according to the model flexible cylinder as previously reported for the C8-dCyt bulk gel.[5] Fitting GISAXS data to a model requires dilute samples[6] that was why the first collected pattern was selected. Grazing Incidence data has been previously fitted to theoretical models to acquire geometrical parameters.[7] The structures of all four gels could be modelled as flexible cylinders with radii of 59.6 ± 0.7 Å, 53.8±1.6, 50.2±0.3 and 61.5±0.3 Å for the C8-dCyt, C10-dCyt, C12-dCyt and C14-dCyt gels, respectively. These radii are considerably larger than the radius of a single fibre formed by the respective gelator, suggesting the presence of fibre bundles as previously reported for the C8-dCyt bulk gel.[5]In accordance with previous literature,[8,9] fibre aggregation due to drying was observed over time on our samples but the effect is not significant at early time-scales (Section 10, SI). Consequently the observed differences in fibre bundle dimensions are related to the different structures of the gelators.

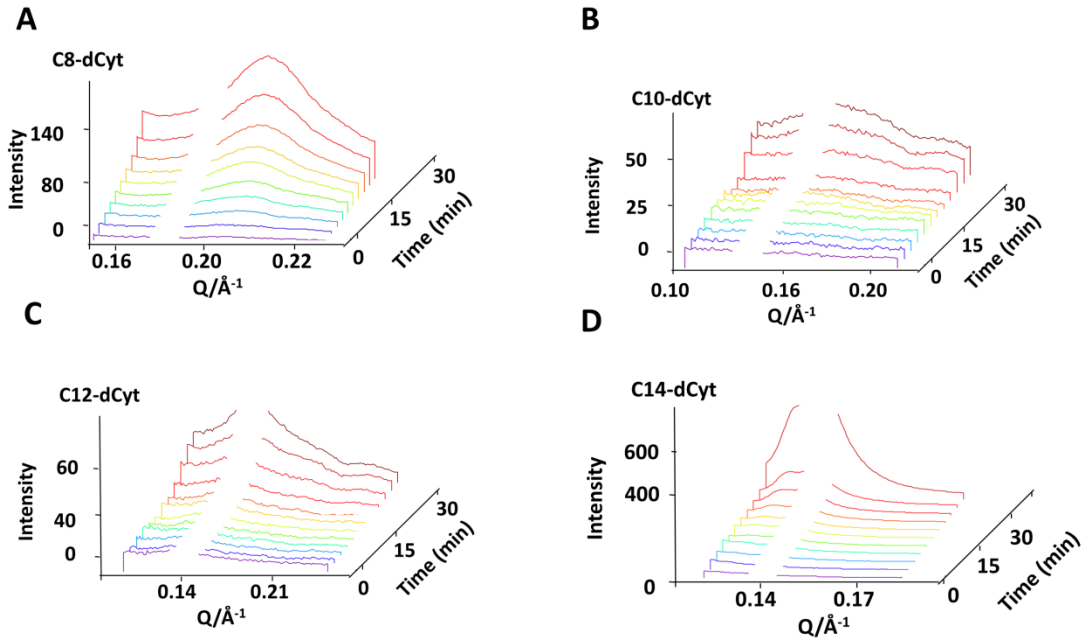

Figure S8: Selected Q-range of time resolved GISAXS patterns of gels formed by for four different cytosine based gelators with varying aliphatic chain lengths on clean silicon wafers ; (A) C8-dCyt, (B) C10-dCyt, (C) C12-dCyt and (D) C14-dCyt. Data points between 0.156 $Å^{-1}$ - 0.158 $Å^{-1}$ are missing due to the spaces between the 2D detector plates.

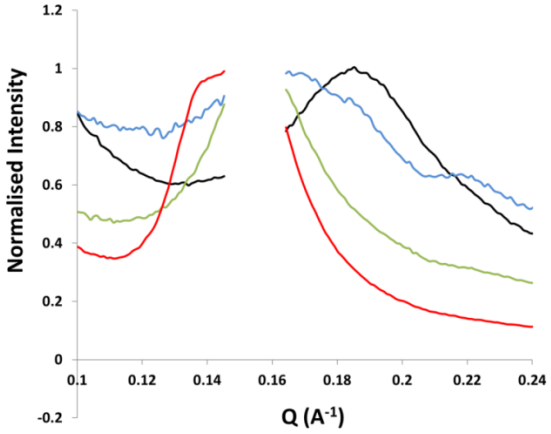

Figure S9: Selected Q-range of GISAXS patterns of dry gels (last pattern collected) formed by four different cytosine based gelators with varying aliphatic chain lengths on clean silicon wafers; C14-dCyt (red trace), C12-dCyt (green trace), C10-dCyt (blue trace) and C10-dCyt (black trace). Data points between 0.156 $Å^{-1}$ - 0.158 $Å^{-1}$ are missing due to the spaces between the detector plates on the 2D detector.

6) Different surface chemistries

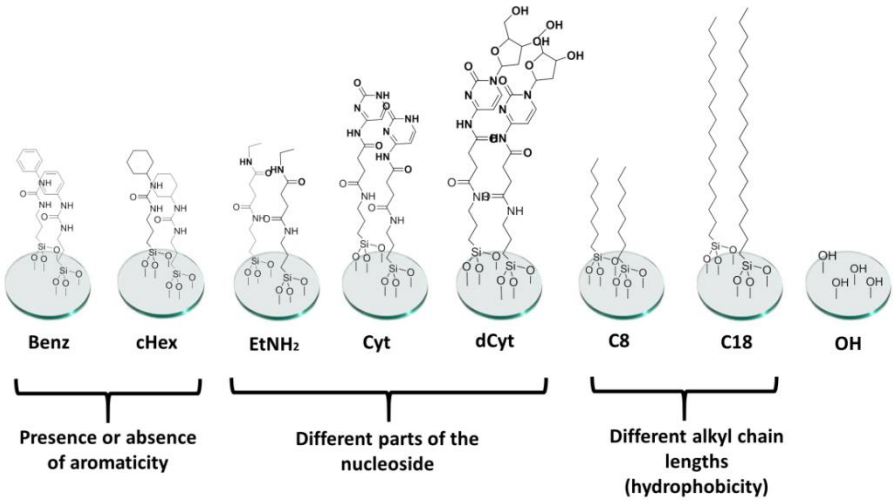

Figure S10: Different chemistries developed and characterised on the silicon wafers and labels used for the different surface chemistries. Different surface chemistries; alkyl chains containing 8 or 18 carbons (C8 and C18), ethylamine ($EtNH_2$), deoxy-cytidine (dCyt), cytidine (Cyt) cyclohexyl (cHex) and benzyl (Benz) groups and piranha cleaned (OH).

7) ToF-SIMS Analysis

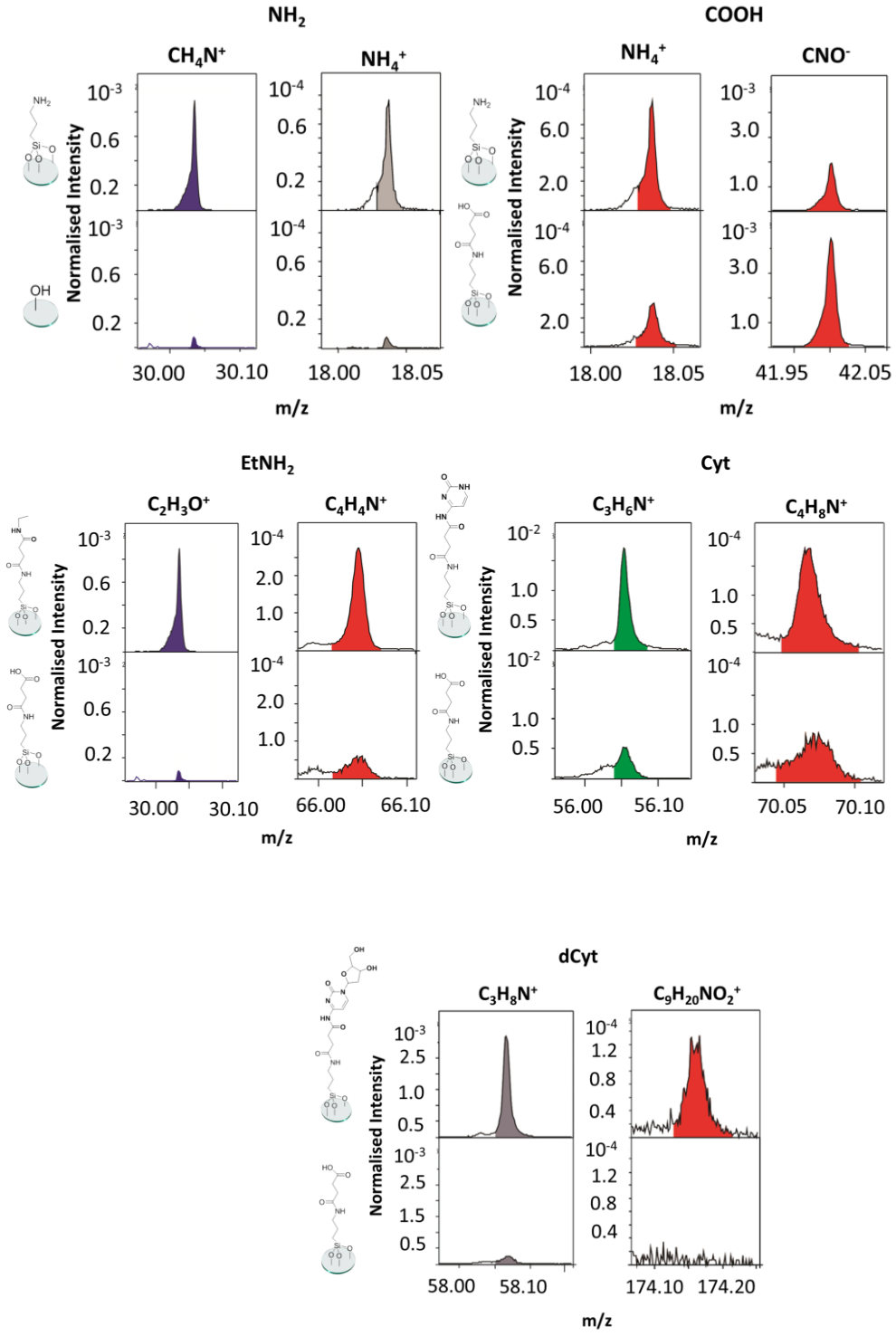

Figure S11: Characteristic ions obtained by ToF-SIMS demonstrating the different chemistries on each surface. Two ions indicative for the annotated surface modification before (bottom) and after (top) the last surface modification step are shown for each surface. Surface chemistries of the relevant samples are shown to the left of the spectra. Different surface chemistries; ethylamine ($EtNH_2$), deoxy-cytidine (dCyt), cytidine (Cyt) cyclohexyl (cHex) and benzyl (Benz) groups and piranha cleaned (OH).

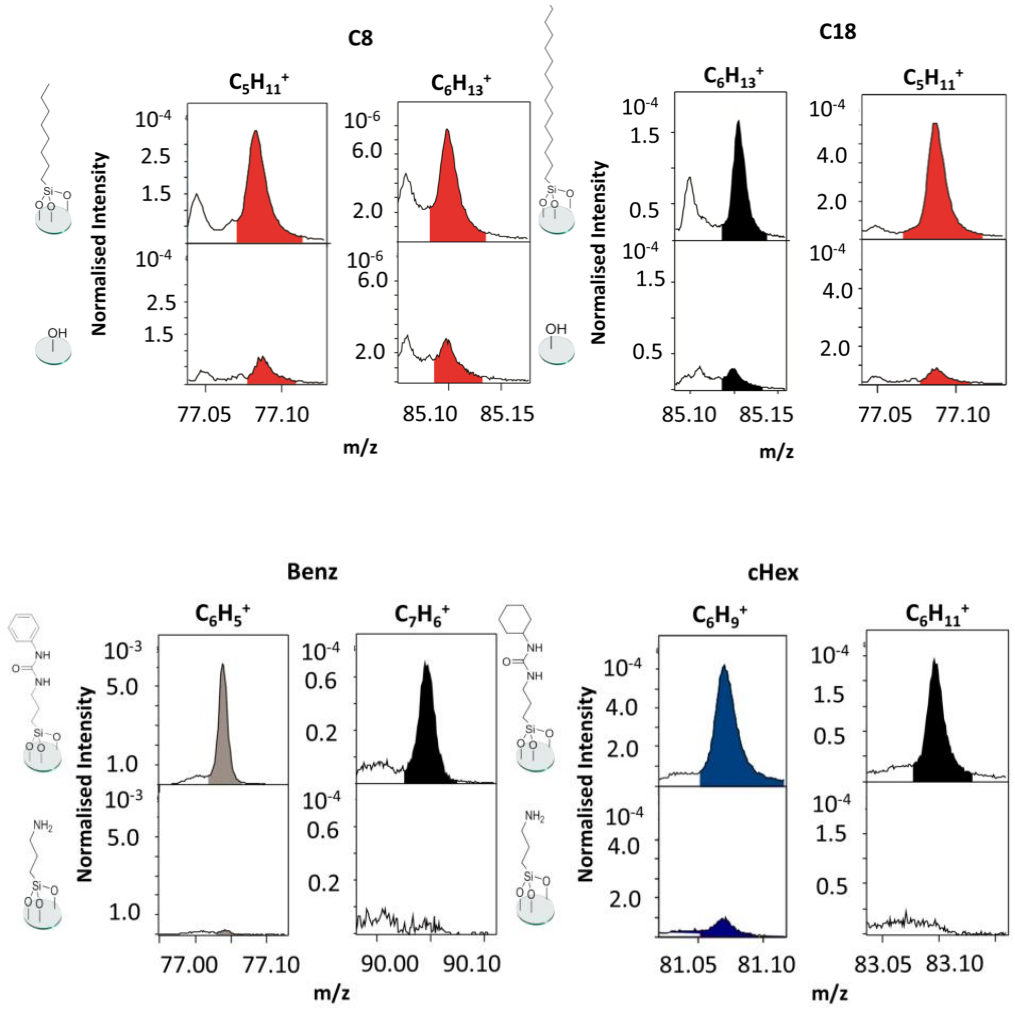

Figure S12: Characteristic ions obtained by ToF-SIMS demonstrating the different chemistries on each surface. Two ions indicative for the annotated surface modification before (bottom) and after (top) the last surface modification step are shown for each surface. Surface chemistries of the relevant samples are shown to the left of the spectra. Different surface chemistries; alkyl chains containing 8 or 18 carbons (C8 and C18), cyclohexyl (cHex) and benzyl (Benz) groups and piranha cleaned (OH).

Table S4: Ions of interest (Figure S11 distribution on four regions of interest (R.O.I.).

NORMALISED INTENSITY FOR IONS (MASS, STANDARD DEVIATION)						
	$C_2O_3^+$ (43.0203, 57.1)		$C_4H_4N^+$ (66.0379, 61.5)		$C_3H_6N^+$ (56.0516,37.1)	
R.O.I.	$EtNH_2$	COOH	$EtNH_2$	COOH	Cyt	COOH
1	3.26E-02	1.58E-02	3.28E-03	1.03E-03	1.98E-02	8.54E-03
2	3.17E-02	1.76E-02	3.42E-03	1.01E-03	1.96E-02	9.06E-03
3	3.78E-02	1.53E-02	3.32E-03	1.31E-03	1.99E-02	7.43E-03
4	3.47E-02	1.87E-02	3.38E-03	1.26E-03	1.98E-02	8.45E-03
mean	0.0342	0.0169	3.40E-03	1.15E-03	1.98E-02	8.37E-03
SD	0.0027	0.0016	6.00E-05	2.00E-04	1.30E-04	6.80E-04
	$C_3H_8N^+$ (58.0672, 35.7)		$H_{20}NO_2^+$ (174.1655,69		$C_4H_8N^+$(70.0654,3.5)	
R.O.I.	dCyt	COOH	dCyt	COOH	Cyt	COOH
1	3.20E-02	4.41E-03	3.07E-04	2.81E-05	3.45E-03	2.04E-03
2	2.92E-02	3.79E-03	2.88E-04	1.10E-05	3.43E-03	2.38E-03
3	3.41E-02	4.84E-03	3.52E-04	2.90E-05	3.52E-03	1.80E-03
4	2.96E-02	4.37E-03	3.07E-04	3.12E-05	3.50E-03	2.13E-03
mean	3.12E-02	4.35E-03	3.13E-04	2.48E-05	3.48E-03	2.09E-03
STD	2.29E-03	4.31E-04	8.00E-05	9.31E-06	4.20E-05	2.40E-04
	CH_4N^+ (30.0331,-25.6)		NH_4^+ (18.0351, 70.7)		NH_4^+(18.0351, 70.7)	
R.O.I.	NH_2	OH	NH_2	OH	COOH	NH_2
1	7.16E-02	8.30E-03	7.08E-03	9.37E-04	0.003491	7.08E-03
2	7.02E-02	6.49E-03	6.68E-03	7.51E-04	0.003344	6.68E-03
3	7.15E-02	8.59E-03	6.72E-03	9.79E-04	0.003594	6.72E-03
4	7.20E-02	4.43E-03	6.62E-03	4.93E-04	0.003489	6.62E-03
mean	7.13E-02	6.95E-03	0.00677	7.90E-04	3.48E-03	6.77E-03
STD	7.80E-04	1.92E-03	0.000206	2.22E-04	1.03E-04	2.06E-04
					CNO- (15.9944, -67.2)	
					COOH	NH_2
					5.08E-02	2.02E-02
					5.10E-02	1.99E-02
					4.90E-02	2.02E-02
					4.97E-02	1.99E-02
					0.050146	2.01E-02
					0.000957	1.60E-04

Table S5: Ions of interest (Figure S12 distribution on four regions of interest (R.O.I.).

NORMALISED INTENSITY FOR IONS (MASS, STANDARD DEVIATION)						
	$C_5H_{11}^+$ (71.0879,33.1)		$C_6H_{13}^+$ (85.1052,47.2)		$C_7H_6^+$ (90.0464, -0.4)	
R.O.I.	**C18**	**OH**	**C18**	**OH**	**Benz**	**OH**
1	6.49E-03	1.93E-03	2.07E-03	6.11E-04	6.81E-02	1.78E-04
2	6.61E-03	2.87E-03	2.05E-03	8.66E-04	6.50E-02	1.58E-04
3	6.37E-03	1.83E-03	2.04E-03	5.94E-04	7.16E-02	1.50E-04
4	6.52E-03	1.26E-03	2.04E-03	3.90E-04	7.15E-02	1.29E-04
mean	6.50E-03	1.97E-03	0.00197	6.15E-04	6.91E-02	1.54E-04
STD	9.90E-05	6.67E-04	0.000667	1.95E-04	3.15E-03	2.00E-05
	$C_6H_9^+$ (81.0699, 46.8)		$C_7H_5^+$ (89.0372, -15.8)		$C_6H_5^+$ (77.0376,-12.8)	
R.O.I.	**cHex**	**OH**	**cHex**	**OH**	**Benz**	**OH**
1	1.21E-02	1.96E-03	1.11E-03	4.13E-04	6.81E-02	3.96E-03
2	1.20E-02	1.96E-03	1.13E-03	4.06E-04	6.50E-02	3.98E-03
3	1.23E-02	1.80E-03	1.35E-03	3.46E-04	7.16E-02	3.58E-03
4	1.22E-02	1.80E-03	1.08E-03	3.42E-04	7.15E-02	3.53E-03
mean	1.22E-02	1.88E-03	1.17E-03	3.77E-04	6.91E-02	3.76E-03
STD	0.000129	9.24E-05	0.000123	3.8E-05	0.003152	0.000241
	$C_5H_{11}^+$(71.0879,-19)		$C_6H_{13}^+$(85.1052,-11.6)			
R.O.I.	**C8**	**OH**	**C8**	**OH**		
1	5.00E-03	2.54E-03	1.38E-03	3.48E-04		
2	4.68E-03	1.59E-03	1.32E-03	5.16E-04		
3	4.76E-03	1.64E-03	1.31E-03	5.08E-04		
4	3.71E-03	1.14E-03	1.03E-03	7.33E-04		
mean	4.54E-03	1.73E-03	1.26E-03	5.26E-04		
STD	5.72E-04	5.85E-04	1.54E-04	1.58E-04		

8) AFM images of xerogels on all the surfaces

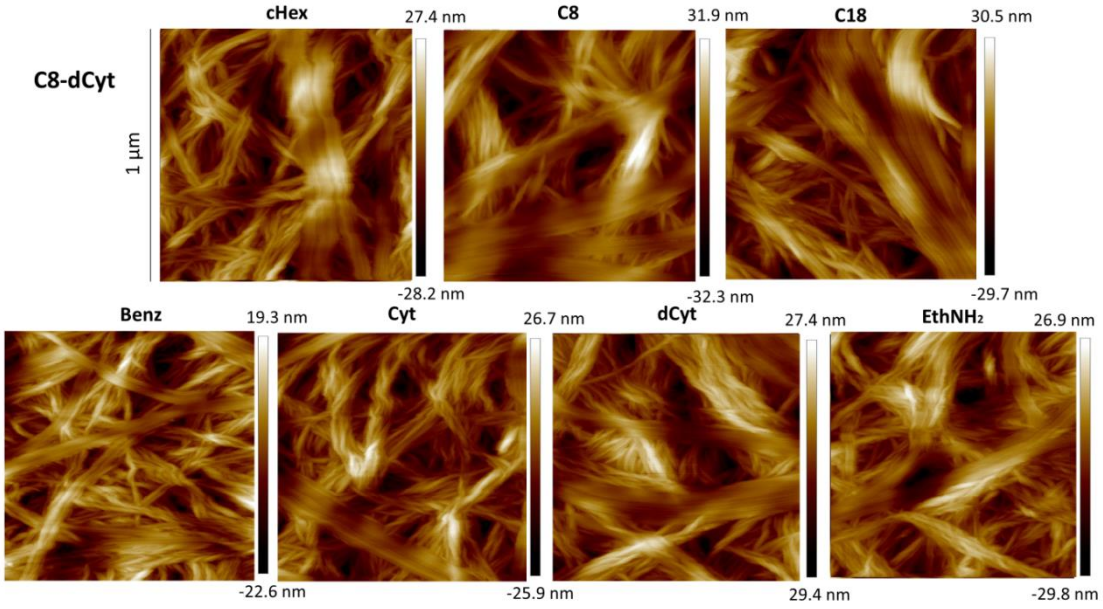

Figure S13: AFM images of gels on different surfaces; gels formed by C8-dCyt on surfaces displaying different chemistries. Different surface chemistries; alkyl chains containing 8 or 18 carbons (C8 and C18), ethylamine ($EtNH_2$), deoxy-cytidine (dCyt), cytidine (Cyt) cyclohexyl (cHex) and benzyl (Benz) groups and piranha cleaned (OH).

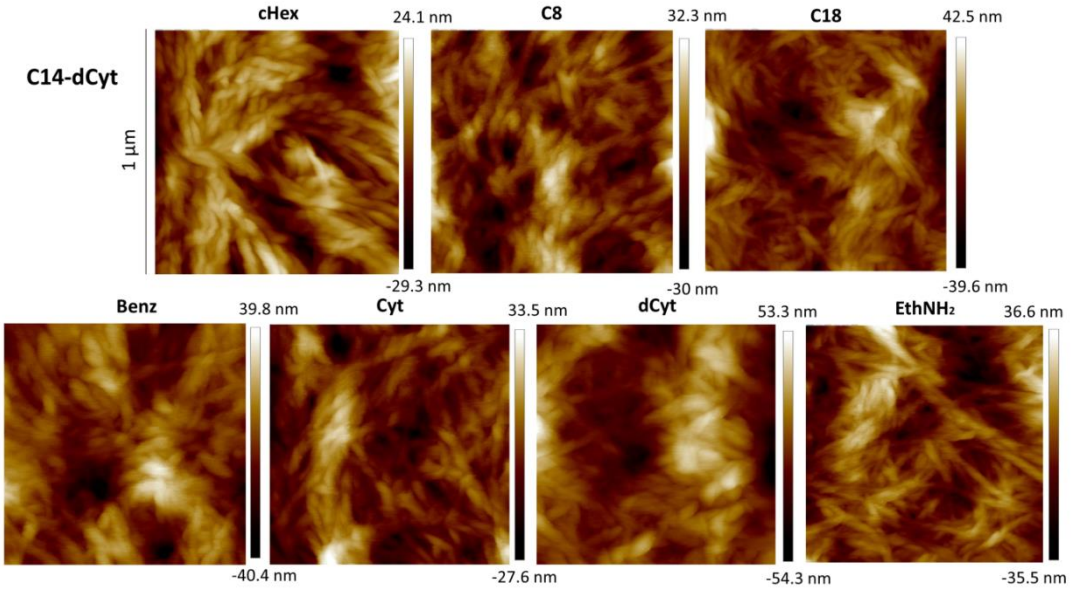

Figure S14: AFM images of gels on different surfaces; gels formed by C14-dCyt on surfaces displaying different chemistries. Different surface chemistries; alkyl chains containing 8 or 18 carbons (C8 and C18), ethylamine ($EtNH_2$), deoxy-cytidine (dCyt), cytidine (Cyt) cyclohexyl (cHex) and benzyl (Benz) groups and piranha cleaned (OH).

9) Linear Regression analyses

Table S6: Independent variables used in the Linear Regression analyses. As independent variables, measured surface parameters (WCA, R_q), theoretical properties of the immobilized molecules (logP, polarizable surface area, calculated by ChemDraw Professional version 16.0) and structural descriptor (number of rotatable bonds, number of aromatic rings) were used

	INDEPENDENT VARIABLES					
property / surface	logP	R_q (nm)	R_a (nm)	WCA (°)	NRB	PSA
Benz	1.675	0.391±0.093	0.195±0.005	57.6±1.2	4	29.1
cHex	2.064	0.676±0.078	0.26±0.021	55.1±1.9	4	29.1
C8	4	0.346±0.035	0.183±0.006	74.7±1.6	5	0
C18	8.558	0.306±0.078	0.228±0.064	72.8±2.7	15	0
$EtNH_2$	-0.034	0.904±0.275	0.659±0.303	67.3±6.5	8	58.2
dCyt	-1.218	1.041±0.092	0.709±0.081	34.5±1.6	10	140.56
Cyt	-0.7	0.698±0.237	0.548±0.208	35.5±1.2	8	99.66
OH	0	1.031±0.167	0.717±0.059	4.7±0.7	0	31.5

Table S7: Dependent variables used in the Linear Regression analyses.

	DEPENDENT VARIABLES	
radius / surface	C14-dcyt	C8-dcyt
Benz	63.768±0.206	75.176±2.5447
cHex	59.008±1.570	63.383±0.11998
C8	55.101±0.44506	59.147±2.7044
C18	41.522±3.4419	56.467±1.348
$EtNH_2$	55.184±3.0752	54.832±0.96758
dCyt	69.127±0.872	64.231±1.6068
Cyt	74.306±0.593	80±0.0000001
OH	61.487±0.30014	59.588±0.654619

Table S8: Statistical output including parameters after testing each idependent variable against a dependent one with Linear Regression analysis.

C14-dCyt	logP	WCA	PSA	NRB	R_q
Best-fit values ± SE					
Slope	-2.813 ± 0.6918	-0.2642 ± 0.1341	0.1626 ± 0.05715	-0.8039 ± 0.8424	17.26 ± 11.68
Y-intercept	65.23 ± 2.592	73 ± 7.381	51.19 ± 4.028	65.15 ± 6.726	48.08 ± 8.538
X-intercept	23.19	276.3	-314.8	81.04	-2.785
1/slope	-0.3555	-3.785	6.151	-1.244	0.05792
95% Confidence Intervals					
Slope	-4.591 to -1.035	-0.5923 to 0.06394	0.01566 to 0.3095	-2.865 to 1.257	-11.32 to 45.85
Y-intercept	58.57 to 71.9	54.94 to 91.06	40.83 to 61.54	48.69 to 81.6	27.19 to 68.97
X-intercept	14.85 to 59.67	149.7 to +infinity	-3749 to -138.3	27.28 to +infinity	-infinity to -0.6093
Goodness of Fit					
R square	0.7678	0.3928	0.6181	0.1318	0.2669
Sy.x	5.742	8.497	7.364	10.16	9.337
Is slope significantly non-zero?					
F	16.53	3.881	8.092	0.9108	2.184
DFn, DFd	1, 5	1, 6	1, 5	1, 6	1, 6
P value	0.0097	0.0963	0.0361	0.3768	0.1899
Deviation from zero?	Significant	Not Significant	Significant	Not Significant	Not Significant
Equation	Y = -2.813*X + 65.23	Y = -0.2642*X + 73	Y = 0.1626*X + 51.19	Y = -0.8039*X + 65.15	Y = 17.26*X + 48.08

C8-dCyt	logP	WCA	PSA	NRB	R_q
Best-fit values ± SE					
Slope	-1.282 ± 1.117	-0.1012 ± 0.1476	0.06881 ± 0.07479	-0.2926 ± 0.7961	-3.156 ± 12.08
Y-intercept	67.32 ± 4.185	69.14 ± 8.123	61.19 ± 5.271	66.03 ± 6.356	66.18 ± 8.83
X-intercept	52.49	683.4	-889.3	225.7	20.97
1/slope	-0.7798	-9.884	14.53	-3.418	-0.3169
95% Confidence Intervals					
Slope	-4.154 to 1.589	-0.4623 to 0.2599	-0.1235 to 0.2611	-2.241 to 1.655	-32.71 to 26.4
Y-intercept	56.56 to 78.08	49.27 to 89.02	47.64 to 74.74	50.48 to 81.58	44.58 to 87.79
X-intercept	17.41 to +infinity	187.4 to +infinity	-infinity to -193.3	35.06 to +infinity	2.614 to +infinity
Goodness of Fit					
R square	0.2087	0.07265	0.1448	0.02201	0.01125
Sy.x	9.27	9.351	9.637	9.603	9.656
Is slope significantly non-zero?					
F	1.318	0.47	0.8464	0.135	0.06825
DFn, DFd	1, 5	1, 6	1, 5	1, 6	1, 6
P value	0.3028	0.5186	0.3998	0.7259	0.8026
Deviation from zero?	Not Significant	Not Significant	Not Significant	Not Significant	Not Significant
Equation	Y = -1.282*X + 67.32	Y = -0.1012*X + 69.14	Y = 0.06881*X + 61.19	Y = -0.2926*X + 66.03	Y = -3.156*X + 66.18

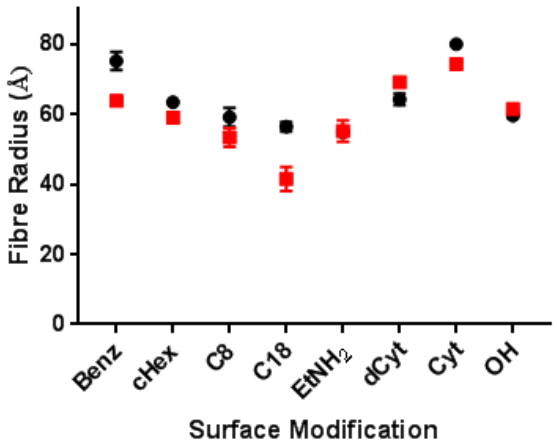

Figure S15: Fibre radii of wet gels on two gelators (black squares (C8-dCyt) red circles (C14-dCyt)) prepared on surfaces with different chemical functionalities obtained from GISAXS data (fitting error is presented for each data point). To compare between the two gelators, Tukey's multiple comparisons test ($P < 0.05$) was performed and no significant difference was observed. Different surface chemistries; alkyl chains containing 8 or 18 carbons (C8 and C18), ethylamine ($EtNH_2$), deoxy-cytidine (dCyt), cytidine (Cyt) cyclohexyl (cHex) and benzyl (Benz) groups and piranha cleaned (OH).

10) Effect of sample drying in data collection and interpretation

Drying has been previously reported to induce fibre aggregation for some gelators,[9] and can contribute the orientation and alignment of gel fibres.[10] Hence the possibility of the presence of drying effects have to be considered in the interpretation of the present data.

The Grazing Incidence geometry used here was operated with an incident angle of 0.08°. This angle is just below the critical angle for the substrate and ensures surface sensitivity. Consequently, the measurements took place on the gel-surface interface rather than the gel-air interface, making the data less susceptible to drying processes that occur at the gel-air interface. To minimise the time between gel application on the surface and the start of the measurement, beam alignment was performed before depositing the gel on the surface and measurements were initiated immediately after gel deposition and collection time for each pattern was 2 seconds, allowing rapid acquisition of the first pattern before drying effects can be established. Higher-order fibre association was then assessed using the first pattern of the time-resolved experiment which corresponds to a wet sample with minimal to no drying effects.

To experimentally demonstrate that drying effects are negligible in the first time-resolved pattern, fibre bundle radii of from the first pattern of gels prepared on piranha cleaned surfaces were compared with those determined for the second pattern (2 minute time interval). Pirhana cleaned surfaces are significantly more hydrophilic than all the other surfaces and the warm solution of the hydrophilic gelator spreads more compared to the rest of the surfaces, resulting in increased surface area exposed to air and thus increased and faster drying effects.

The radii acquired for were; 59.588 ± 0.654619 Å (0 min) and 60.363 ± 0.19862 Å (2 min) for C8-dCyt and 61.487 ± 0.30014 Å (0 min) and 61.302 ± 0.14393 Å (2 min) for C14-dCyt (fitting parameters are presented in Table S10). This demonstrate that the fitted radii did not change within the course of the two first minutes and drying effects are negligible when the first time-resolved patterns are compared. Drying effects can therefore not explain differences in the first patterns observed between samples.

11) Fitting approach GISAXS

The first pattern collected from GISAXS data was fitted using SasView-4.1 to the Kratky-Porod flexible cylinder model (Figure S16) and an example fitting is presented in Figure S17.[11,12] SAXS in the GI geometry have been previously fitted as reported in the literature using theoretical models.[7]

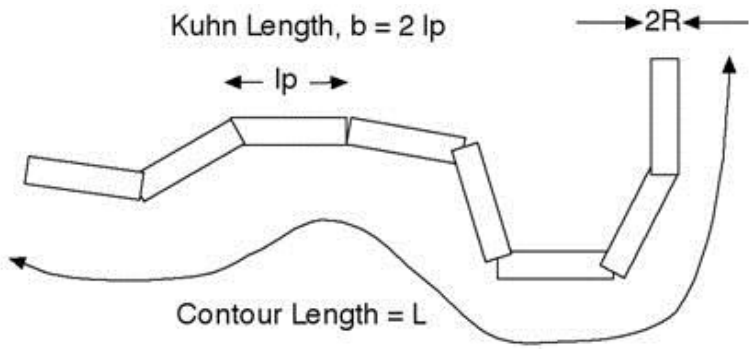

Figure S16: Schematic representation of Kratky-Porod flexible cylinder model used as a fitting model for the GISAXS data.

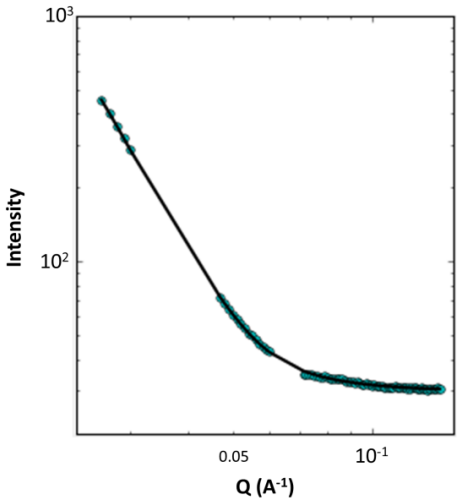

Figure S17: Representative GISAXS pattern of wet C8-dCyt gel on OH surface, the solid line on the pattern is a fit to the data with a Kratky-Porod flexible cylinder model. Data points between 0.030 $Å^{-1}$ - 0.048 $Å^{-1}$ and 0.062 $Å^{-1}$ - 0.074 $Å^{-1}$ are missing due to masking by the reflective beam-stop and the spaces between the detector plates, respectively.

Table S9: The model fit parameters generated by fitting the GISAXS pattern of gels formed on the different surfaces with a Kratky-Porod flexible cylinder model in the SasView-4.1 analysis package.

Gelator	C8-dCyt	C10-dCyt	C12-dCyt	C14-dCyt
	OH	OH	OH	OH
Scale	5.9825±0.095376	2.0175±0.0093582	1.8541±0.015445	10.817±0.050224
Background	29.832	20.947	27	33
Length	1.2335E+32±3.5738E+33	507.69±32.474	3.79E+15±6.58E+15	1.32E+05±6.78E+04
Kuhn length	98.193±0.6364	131.31±1.5796	98.982±1.2874	134.63±4.2096
Radius	59.588±0.654619	53.829±1.6456	50.206±0.29695	61.487±0.30014
Schulz distribution of radius	0.29679±0.022256	0.89783±0.0073768	0.000001439±0.0036674	0.46187±0.0013729
Chi^2/Npts	0.13	1.12	3.5	1.87

Table S10: The model fit parameters generated by fitting the GISAXS pattern of gels formed on the different surfaces with a Kratky-Porod flexible cylinder model in the SasView-4.1 analysis package.

Gelator	C14-dCyt				
	Benz	cHex	dCyt	Cyt	EtNH2
Scale	13.245±0.064	2.052±0.396	5.272±0.024	2.057±0.011	1.7257±0.096
Background	37.231	42.562	37.33	41.45	23.038
Length	33650±8040	1.40E+14±6.65E+14	8.10E+41±7.68E+41	1.55E+44±1.61E+44	7.50E+24±1.00E+08
Kuhn length	63.443±2.160	105.36±8.09	111.06±1.1449	116.17±1.2031	112±7.3625
Radius	63.768±0.206	59.008±1.570	69.127±0.872	74.306±0.593	55.184±3.0752
Schulz distribution of radius	0.382±0.005	0.267±0.042	0.600±0.005	0.365±0.005	0.35756±0.0419
Chi^2/Npts	0.3	0.7	0.3	0.4	0.05
Gelator	C14-dCyt			C8-dCyt	
	C8	C18	OH	C8	C18
Scale	2.5396±0.011745	1.0761±0.14233	10.817±0.050224	5.8076±0.20967	4.3451±0.48517
Background	43.669	48.47	33	33.54	26.986
Length	5.47E+35±4.69E+35	4.01E+02±5.29E+03	1.32E+05±6.78E+04	8.17E+10±1.00E+08	5.67E+20±1.58E+22
Kuhn length	75.939±0.50502	100.37±15.404	134.63±4.2096	53.808±4.2126	102.62±6.2522
Radius	55.101±0.44506	41.522±3.4419	61.487±0.30014	59.147±2.7044	56.467±1.348
Schulz distribution of radius	0.20079±0.0066877	0.60371±0.038536	0.46187±0.0013729	0.63497±0.52347	0.041355±0.02275
Chi^2/Npts	1.7	1.2	1.87	0.64	0.013
Gelator	C8-dCyt				
	Benz	cHex	dCyt	Cyt	OH
Scale	15.815±0.76759	13.146±0.54997	11.937±0.37097	15.425±1.004	5.9825±0.095376
Background	32.644	29.783	29.878	31.779	29.832
Length	9.53E+08±1.47E+10	1.10E+22±1.00E+08	3.55E+12±1.00E+08	1.06E+46±2.01E+47	1.2335E+32±3.5738E+33
Kuhn length	117.42±5.3623	101.78±3.5611	107.51±3.6385	107.34±1.5184	98.193±0.6364
Radius	75.176±2.5447	63.383±0.11998	64.231±1.6068	80±0.00000010937	59.588±0.654619
Schulz distribution of radius	0.38466±0.0045008	0.39587±0.33032	0.37619±0.0063078	0.51276±0.04749	0.29679±0.022256
Chi^2/Npts	7.2	3.5	1.1	4	0.13

Gelator	C8-dCyt
	$EtNH_2$
Scale	3.7907±0.1297
Background	63.463
Length	5.01E+9±1.00E+08
Kuhn length	61.807±4.7398
Radius	54.832±0.96758
Schulz distribution of radius	0.63757±0.041084
Chi^2/Npts	1.5

Table S11: The model fit parameters generated by fitting the GISAXS pattern of gels formed on the OH surfaces at 0 min and 2 min with a Kratky-Porod flexible cylinder model in the SasView-4.1 analysis package.

Gelator	C14-dCyt - OH surface	
	0 min	**2 min**
Scale	10.817±0.050224	23.736±0.026
Background	33	33
Length	1.32E+05±6.78E+04	2.36E+37±5.57E+36
Kuhn length	134.63±4.2096	112.74±0.477
Radius	**61.487±0.30014**	**61.302±0.144**
Schulz distribution of radius	0.46187±0.0013729	0.42408±0.001
Chi^2/Npts	1.87	3.8
Gelator	C8-dCyt - OH surface	
	0 min	**2 min**
Scale	5.9825±0.095376	8.778±0.02839
Background	29.832	32.14
Length	.2335E+32±3.5738E+3	3.96E+38±3.258E+38
Kuhn length	98.193±0.6364	94.804±1.029
Radius	**59.588±0.654619**	**60.363±0.19862**
Schulz distribution of radius	0.29679±0.022256	0.30879±0.001098
Chi^2/Npts	0.13	1.65

12) Synthesis and characterisation of the gelators

The four different gelators were synthesized according to the protocol published before[13] and characterisation data are presented below.

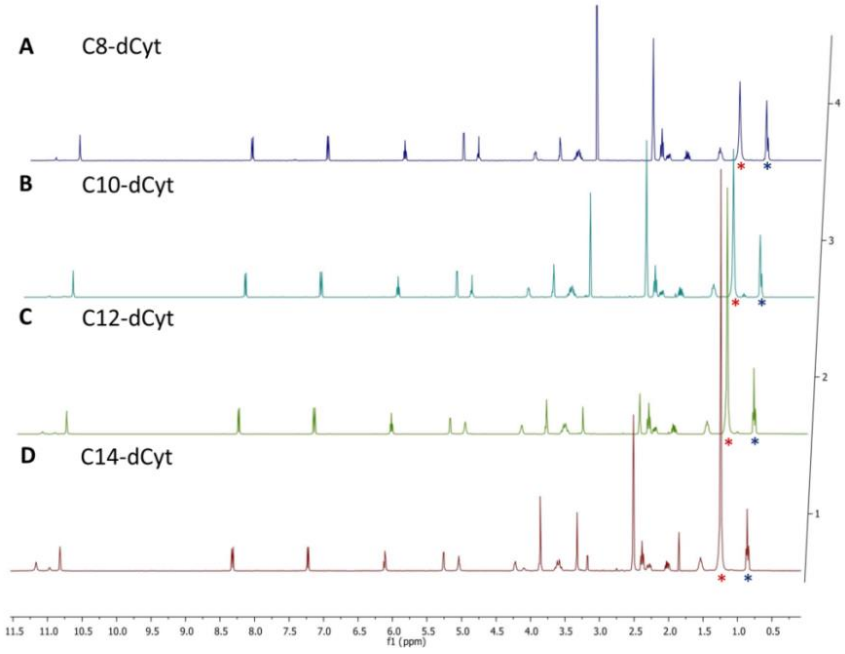

Figure S18: ^{1}H NMR traces for the four different gelators, demonstrating the similarity in the structures of the four molecules. The peak intensities are normalised to the peak at δ 0.86 (3H, $\underline{CH_3}$) of C8-dCyt (blue asterisk) confirming the difference in the alkyl chain lengths when compared to the peak at δ~1.25 (CH_2-($\underline{CH_2}$)$_x$-CH_3) with x = 20 hydrogen atoms for C14-dCyt, x=16 for C12-dCyt, x=12 for C10-dCyt and x=8 for C8-dCyt (red asterisk). Spectra have been setoff to demonstrate the difference in the relative intensities. Spectra have been assigned in detail in previously published work.[13]

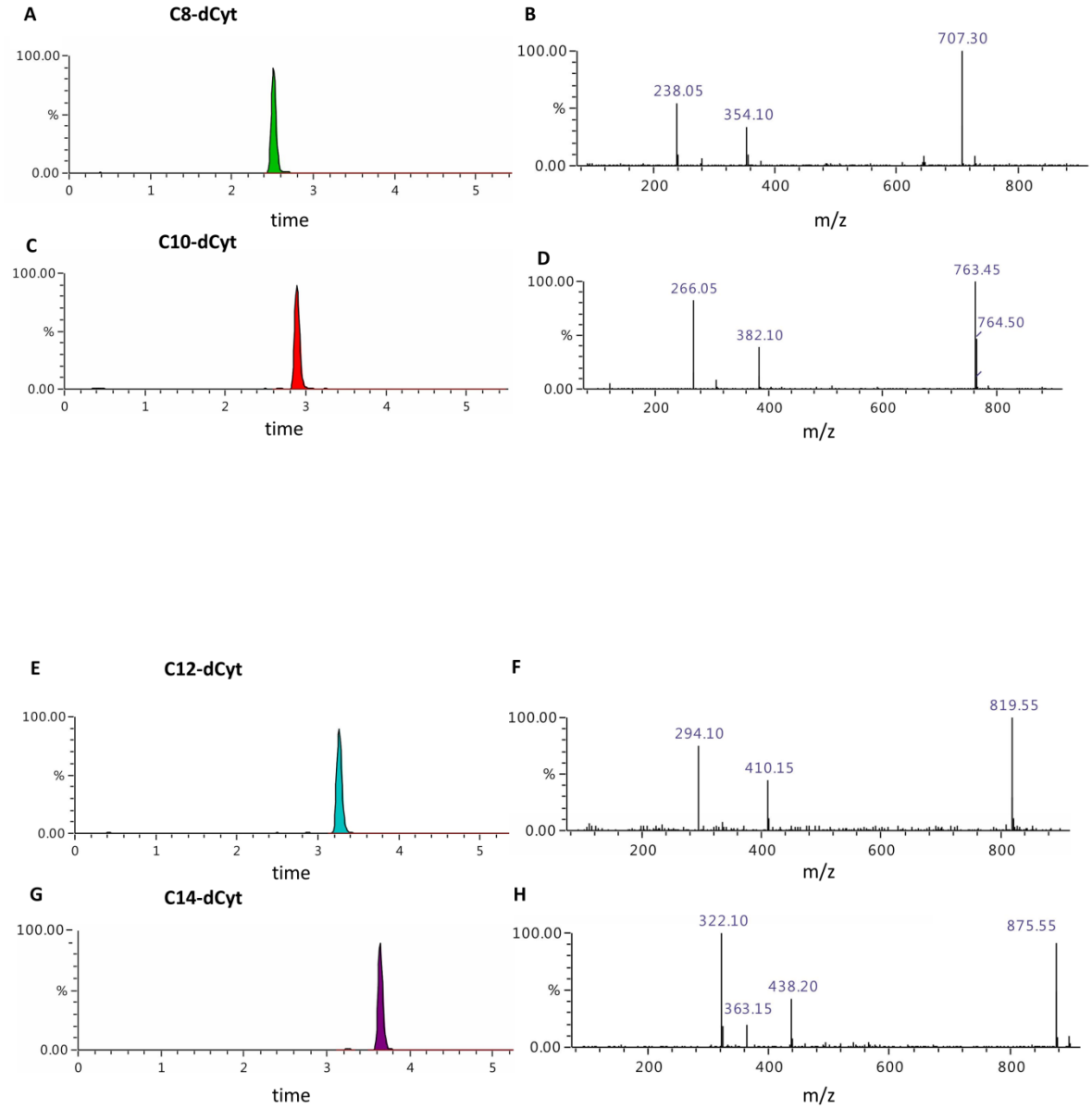

Figure S19: LC-MS analysis of different gelators in methanol. Purity determined from the chromatogram as >99% (by height) and >98% (by area) by UV at 254 nm for (A) C8-dCyt, (C) C10-dCyt, (E) C12-dCyt and (G) C14-dCyt. MS (+) spectrum with main ions detected for (B) C8-dCyt at m/z 238.05 [N_4 -octanoylcytosine + H]$^+$, 354.10 [M+H]$^+$ and 707.30 [2M + H] $^+$, (D) C10-dCyt at m/z 266.05 [N_4 -decanoylcytosine + H]$^+$, 382.10 [M+H]$^+$ and 763.45 [2M + H] $^+$,(F) C12-dCyt at m/z 294.10 [N_4 -dodecanoylcytosine + H]$^+$, 410.15 [M+H]$^+$ and 819.55 [2M + H] $^+$, (H) C14-dCyt at m/z 322.10 [N_4 -tetradecanoylcytosine + H]$^+$, 438.20 [M+H]$^+$ and 875.55 [2M + H] $^+$,

13) Experimental methods

13.1) Materials

2'-Deoxycytidine [lot #SLBN6031, 99% [high-performance liquid chromatography (HPLC)] was purchased from Sigma Aldrich. All the gelators were synthesized according to procedures reported previously.[13] Solvents (HPLC grade) were obtained from Fischer Scientific. Analysis of the gelator was performed by NMR and liquid chromatography–mass spectrometry (LC–MS) (Supporting Information Figures S18, S19), and purity was determined as >98% (LC–MS). Silicon Wafers - Reclaim Grade P(Boron) (PI-KEM Limited, Product Code: SILI0029W), 4" Diameter,425-550 µm thick, P(Boron), 0-100 ohm cm, Single Side Polished. (3-Aminopropyl)trimethoxysilane, 97% (Alfa Aesar, product code: A1128422)Sulphuric acid 95-97% w/v BP analytical grade was purchased from Sigma Aldrich. Hydrogen peroxide 100 volumes >30% w/v laboratory reagent grade were purchased from Fisher Chemicals. Methanol HPLC grade, Acetone HPLC grade, Propan-2-ol analytical reagent grade, Toluene analytical reagent grade were purchased from Fischer Chemicals UK. water used was milli Q (18.2 MΩ·cm) ultrapure water DIC purum, ≥98.0% (GC) (Sigma-Aldrich, product code: 38370).N,N-Dimethylformamide anhydrous, 99.8% (Sigma-Aldrich, Product code: 227056). Triethylamine, ≥ 99.5% (Sigma-Aldrich, Product code: 471283). n-Octyltrimethoxysilane, 97+% (Alfa Aesar, Product code: 42698). Trimethoxy(octadecyl)silane technical grade, 90% (Sigma Aldrich, Product code: 376213).Succinic anhydride≥99% (GC), (Sigma Aldrich, product code: 239690).Cyclohexanecarboxylic acid, 98% (Product code: 101834). Benzoic acid ACS reagent, ≥99.5% (Product code: 242381).

13.2) Surface modification

To create the differently modified surfaces, cleaned silicon wafers were used as substrates. The samples were placed in petri dishes and cleaned by sequentially sonicating them for five minutes in methanol, acetone and isopropanol. The substrates were then dried using compressed air and clean, hydrophilic surfaces covered with hydroxyl groups were accomplished via piranha cleaning. 30 ml Piranha solution of 1:3 of H_2O_2/H_2SO_4 was added to a glass petri dish containing the samples and left for 30 minutes. The samples were rinsed with Millipore ultrapure water and dried with compressed air.

The synthetic pathways for all surfaces are presented in Figure S20 Amine terminated surfaces (NH_2) were generated via silanisation of the slides with (3-aminopropyl) trimethoxysilane (APTMS). The slides were incubated in a glass petri dish in 20 ml of a 1 % solution of APTMS in toluene at room temperature for 1 hour, followed by washing with toluene, acetone and Millipore ultrapure water and drying under compressed air.

To immobilise different parts of the nucleoside, amino-terminated surfaces (NH_2) were incubated in a glass petri dish in 15 ml of anhydrous DMF with 1.5 g succinic anhydrite and 20 µl of trimethylamine at room temperature overnight and then rinsed with DMF, acetone, methanol and water to produce carboxylic acid-terminated surfaces (COOH). In the last step of the modification the carboxylic acid terminated surfaces prepared before were incubated overnight in a glass petridish in 15 ml of DMF and 90 µl of diisopropylcarbodiimide (DIC) with 20 mM of 2'-deoxycytidine (for the deoxycytidine terminated surfaces, dCyt) and ethylamine hydrochloride (ethylamine-terminated surfaces, $EtNH_2$) at room temperature overnight. For the cytosine- terminated surfaces (Cyt), we incubated overnight in a glass petridish in 15 ml of anhydrous DMSO and 90 µl of diisopropylcarbodiimide (DIC) with 20 mM of cytosine at room temperature overnight. For the cyclohexane- and benzene- terminated surfaces, the amino-terminated surfaces were incubated in

15 ml of anhydrous DMSO with 90 µL DIC and 20 mM of cyclohexanoic acid and benzoic acid at room temperature overnight. The different alkyl terminated surfaces were incubated in 25 ml of toluene 5% *n*-octyltrimethoxysilane and *n*-octadecyltrimethoxysilane at 70 ˚C for 1 h. When at room temperature surfaces were shaken on a Heidolph Rotamax 120 Orbital Shaker at 20 rpm for 16 hours. After incubation, the slides were rinsed in the solvent of incubation, methanol, acetone and Millipore water.

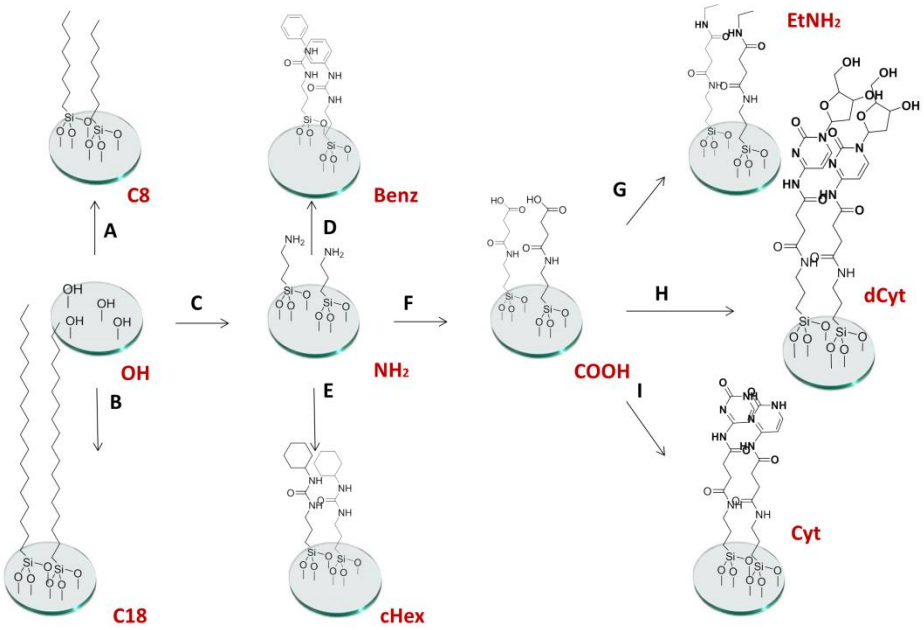

Figure S20: Synthetic pathways for the different surfaces. Piranha cleaned surfaces were incubated in 25 ml of toluene 5% v/v (A) n-octyltrimethoxysilane and (B) n-octadecyltrimethoxysilane at 70 ˚C for 1 h. (C) Piranha cleaned surfaces were incubated in 1 % v/v with (3-aminopropyl) trimethoxysilane (APTMS) in toluene at room temperature for 1 h. (F) Amino-terminated surfaces were incubated in 15 ml of anhydrous DMF with 1.5 g succinic anhydrite and 20 µl of trimethylamine at room temperature overnight. In the last step of the modification the surfaces prepared before we incubated overnight in glass petridish in 15 ml of DMF AND 90 µl of diisopropylcarbodiimide (DIC) with 20 mM of (H) 2'-deoxycytidine and (G) ethylamine hydrochloride at room temperature overnight. (I) Carboxy-terminated surfaces in 15 ml of anhydrous DMSO and 90 µl of diisopropylcarbodiimide (DIC) with 20 mM of cytosine at room temperature overnight. For the cyclohexane and benzene- terminated surfaces the amino-terminated surfaces were incubated in 15 ml of anhydrous DMSO with 90 µL DIC and 20 mM of (E) cyclohexanoic acid and (D) benzoic acid at room temperature overnight.

13.3) Surface characterisation

13.3.1) Water Contact Angle (WCA) measurements

Water contact angle (WCA) measurements were used to monitor changes in surface properties. The WCA was determined with a KSV Cam200 Optical Contact Angle Meter. The Cam200 was set up to record 10 frames at a speed of one frame per second for each droplet. The WCA of the droplet in each frame were then calculated using the circle fitting method by Cam200. The first two values

were excluded and the other eight were averaged. The WCA measurements are presented as average ± standard deviation (SD).

13.3.2) ToF-SIMS analysis

ToF-SIMS analysis was performed using an ION-TOF TOF-SIMS IV instrument (Münster, Germany). 3 mm x 3 mm raster scans (with 256 x 256 pixels) were obtained using 25 keV Bi_3^+ primary ions with charge compensation. The data was analysed with Surfacelab 6. Positive ion mass spectra were calibrated with m/z 1 (H^+), 15 (CH_3^+), 29 ($C_2H_5^+$), 43 ($C_3H_7^+$) and 57 ($C_4H_9^+$). Spectra were manually analysed and major peaks were identified and assigned to mass fragments by the software algorithm. The analysed areas were divided into four 1.5 mm x 1.5 mm quadrants. For each quadrant, the area under the curve for ions of interest was determined and normalized to the total ion intensities (ESI Table S3).

13.3.3) Atomic Force Microscopy Imaging

The modified cover glass with and without gels were imaged using a Bruker AFM Probe D300 atomic force microscope in tapping mode (75 kHz, spring constant 3 N/m, cantilever thickness: 3 µm, scan rate: 0.5 Hz, target amplitude: 3.0 V). Each image consists of 512 line scans. At least one AFM image was obtained from each of the three repeat samples that were prepared for each gelator/surface combination.

14) References

1. Allain, Bourgaux and Couvreur, *Nucleic acids research*, 2011, **40**, 1891-1903.
2. Aggeli, Nyrkova, Bell, Harding, Carrick, McLeish, Semenov and Boden, *Proceedings of the National Academy of Sciences*, 2001, **98**, 11857-11862.
3. Nuthanakanti and Srivatsan, *Nanoscale*, 2016, **8**, 3607-3619.
4. Peters and Davis, *Chemical Society Reviews*, 2016, **45**, 3188-3206.
5. Angelerou, Frederix, Wallace, Yang, Rodger, Adams, Marlow and Zelzer, *Langmuir*, 2018.
6. Guilbaud and Saiani, *Chemical Society Reviews*, 2011, **40**, 1200-1210.
7. Hsu, Jeng, Lee, Huang, Liang, Windover, Lu and Jin, *Thin Solid Films*, 2005, **472**, 323-327.
8. Adams, *Gels*, 2018, **4**, 32.
9. Mears, Draper, Castilla, Su, Dietrich, Nolan, Smith, Doutch, Rogers, Akhtar, Cui and Adams, *Biomacromolecules*, 2017, **18**, 3531-3540.
10. Wang, Lei, Luo, Cai, Li, Cheng, Zhuo and Zhang, *Langmuir*, 2013, **29**, 6996-7004.
11. Pedersen and Schurtenberger, *Macromolecules*, 1996, **29**, 7602-7612.
12. Chen, Butler and Magid, *Langmuir*, 2006, **22**, 6539-6548.
13. Skilling, Kellam, Ashford, Bradshaw and Marlow, *Soft Matter*, 2016, **12**, 8950-8957.